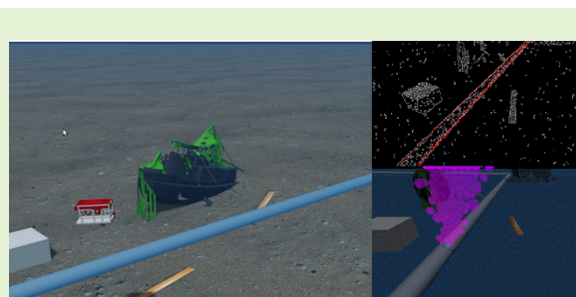# An Autonomous Underwater Vehicle Simulation with Fuzzy Sensor Fusion for Pipeline Inspection

I-Chen Sang , William R. Norris

Abstract— **Underwater pipeline inspection is an important topic in off-shore subsea operations. ROVs (Remotely Operated Vehicles) can play an important role in multiple application areas including military, ocean science, aquaculture, shipping, and energy. However, using ROVs for inspection is not cost-effective, and the fixed leak detection sensors mounted along the pipeline have limited precision. Although the cost can be significantly reduced by applying AUVs (Autonomous Underwater Vehicles), the unstable current, low visibility and loss of GPS signal make the navigation of AUVs underwater very challenging. Previous studies have been conducted on coordinate-based, vision-based, and fusion-based navigation algorithms. However, the coordinate-based algorithms suffered from the denial of GPS signals while the vision-based methods typically relied on terrain and landscape knowledge that required collection prior to the mission. As a result of these issues, a navigation system for an AUV (Autonomous Underwater Vehicle) that incorporates vision and sonar sensors is presented in this paper. In a ROS/Gazebo-based simulation environment, the AUV had the ability to find and navigate towards the pipeline and continuously traverse along its length. Additionally, with a chemical concentration sensor mounted on the AUV, the system demonstrated the capability of inspecting the pipeline and reporting the leak point with a resolution of 3 meters along the pipeline.**

Index Terms— **Autonomous Underwater Vehicle, Fuzzy Controller, Pipeline Inspection, ROS, Sensor Fusion, Simulation**

I. INTRODUCTION

A. Motivation

UNDERWATER pipelines are essential infrastructure for the transportation of oil and gas. However, cracks are likely to be found on pipelines due to the extreme marine environments. Furthermore, underwater pipelines become more vulnerable as they age, thereby exposing them to more damage [1]. Gas and oil leaks, and other forms of ocean pollution caused by pipeline systems are extremely expensive to repair and negatively impact fuel reserves. As a result, periodic inspection of underwater pipelines is a necessary and important issue in oceanic engineering.

Before the development of advanced autonomous vehicle technology, pipeline inspections were primarily performed using visual inspection and sensor networks [2]. Visual inspections are carried out by examining close-up images collected by divers or ROVs. Fluorescent dyes could be added to raise the accuracy of the leak detection. Apart from visual

inspections, acoustic sensors or chemical sensors installed along the pipelines could indicate the presence of a leak [3]. When detecting a leak, a signal is sent either through the network, or to cruising ROVs [4]. These approaches have several weaknesses as sensor networks are vulnerable and have limited precision due to the distance between sensors. In addition, the power required for a sensor or receiver network increases complexity for the whole system.

ROVs and AUVs were introduced to the field of underwater pipeline inspection in order to overcome precision and mobility issue. [5] Among the two options, AUVs outperform ROVs due to better automation and reduced workforce requirement.It was first proposed in [6], that inspections can be performed by Autonomous Underwater Vehicles (AUVs) with predefined task flows. After finding the pipeline, AUVs can navigate along the pipeline to conduct the inspection mission.

Despite the improvements made possible by AUVs, the highly complicated environment underwater makes the navigation of AUVs extremely challenging. For example, limited access to GPS signals significantly constrains localization precision. Low visibility and shadows add to the complexity of capturing and interpreting vision-related data. Moreover, the current flow and disturbances pose an even greater challenge to controlling AUVs.

The goal of this study was the development of a navigation algorithm that can overcome the difficulties mentioned above. Under a GPS-denied environment with typical sea currents

and limited visibility, the algorithm is expected to navigate the AUVs to follow the pipeline and conduct leak detection tasks.

B. Related Work

There have been many studies exploring the navigation of an AUV along pipelines [7]. One of the popular approaches has been to save the coordinates along the pipeline, and use the current AUV position for navigation [8] [9]. Reinforcement learning [10] and fuzzy logic [11] [12] were used for increased precision. However, due to the lack of GPS signals and drift in inertial sensing, the precision of coordinate-based methods was limited.

In order to overcome the GPS issue in coordinate-based navigation, the vision-based approach was widely used to assist the systems. Given the limited visibility in this simulation, navigation methods using natural landscapes as references were excluded due to the extended distances. The systems searched for features from nearer objects, such as the seabed [13], artificial landscapes [14], or the pipeline. A common approach involved extracting underwater pipelines from images using edge detection algorithms [15] [16] [17] [18]. Learning-based models were used to translate the acquired image into corresponding control commands. [19]. However, the reliabilities of vision-only approaches were dominated by visibility, and the difficulties in acquiring underwater datasets. [20].

Sonar images from scanning sonar sensor arrays have been commonly used in AUV navigation in order to overcome the visibility issues. Thus, similar edge detection techniques could be applied toward sonar images to localize along the pipeline [21] [22] [23] [24]. Semi-automated pipeline inspection using scanning sonar sensors has been introduced into the market as they are not limited by underwater visibility. However, the cost of sonar array sensors is much higher than RGB cameras.

The research community has been exploring potential solutions combining the vision-only and sonar-only approaches given the advantages and disadvantages previously discussed. Sensor fusion is the most promising approach for providing robust vision-only navigation methods [25]. Underwater camera information can be fused with various sensors for navigation purposes.

The fusion of the camera with other sensors has been used in a variety AUV general localization studies. Karras et al used the fusion result of the Inertial Measurement Unit (IMU) and a downward-looking camera to obtain the position of the AUV [26]. Billings et al combined a stereo camera and a fish-eye camera to construct a SLAM (simultaneous localization and mapping) structure [27]. Similarly, Vargas et al incorporated acoustic odometry with an onboard camera for a robust SLAM algorithm.

In the field of underwater pipeline inspections, few attempts of applying sensor fusion have succeeded. Acosta et al combined detection results from the multi-beam sonar and magnetometer to follow a pipeline [28]. The studies performed by Jacobi et al [6] [25] proposed a pipeline inspection framework incorporating cameras, multi-beam echo sounders, sub

bottom profilers, and magnetic sensors. A probability map was generated by combining the detection result of all the sensors. The result demonstrated successful map construction, but there were no navigation experiments.

C. Contribution and overview of the study

A fuzzy control method for fusing image and sonar data is presented in this study in order to achieve higher levels of reliability and lower cost. Instead of using side-scan sonar, a 4-unit sonar sensor was utilized to lower the cost. Moreover, with the pipeline detection algorithm in this study, a predetermined map of the terrain and others features was not required. The navigation method enabled the AUV to successfully cruise along the pipeline and simultaneously report the chemical concentration in the simulation environment.

In verifying the proposed framework, experiments were conducted in a simulation environment including complications from limited visibility and shadows. The experiments demonstrated that even without access to GPS signals, the algorithm could navigate the AUV to follow the underwater pipeline and detect leaks in the pipeline with a precision of 3m.

The remainder of this paper describes a method, result and conclusion for the study. All theoretical derivation and experimental setup are illustrated in detail in section II. The errors from the pipeline detection, navigation and during leak detection are all presented in section III. The conclusion of the proposed study and several potential future research topics are proposed in section IV.

II. METHOD

The proposed algorithm integrated vision and sonar data, enabling precise path following without access to GPS data. By interpreting vision and sonar data into navigation error measurements, the fuzzy controller was leveraged to make the proper decision and control the propellers.

The validation of the proposed algorithm was done under a simulation framework where all physical properties were simulated and captured. It was shown that the AUV could successfully approach the underwater pipeline, follow it precisely, and identify the leak point simultaneously. In this section, the simulation environment, navigation algorithm, leak detection algorithm and grid map construction methods are described respectively.

A. Simulated Environment

1) Physical properties simulation: A simulation environment [29] based on ROS/Gazebo platform was adopted to verify the proposed algorithm. As Gazebo did not have a default underwater model available, an "Ocean box" model simulated the role of the ocean.

The attenuation of light over depth, distance, and wavelengths were included in the simulation. The exponential attenuation followed the equation

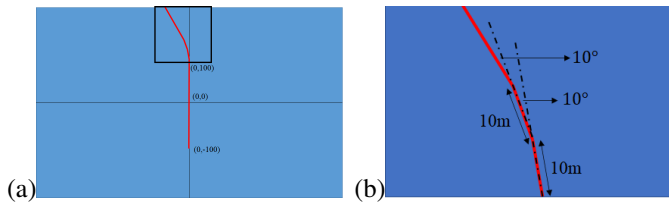$$i_{c,m} = i_c e^{-ra_c} + (1 - e^{-ra_c})b_c \tag{1}$$

Fig. 1. Size and position setup of the underwater pipeline (a)global view (b)detailed view in the turning point (the marked box in (a))

where c was the notation of the channel (R,G,B). i_c and $i_{c,m}$ were the intensity value of channel c before/after the attenuation. b_c was the background intensity. r was the distance to the object, and a_c was the attenuation factor of each channel. In the default setting of the simulator, 0.1/0.1/0.03 represented a_c in red/green/blue respectively. The system noise was added to the camera by post-processing the data. Moreover, shadow was also made visible, which helped in simulating real world issues such as locating the pipeline with cameras.

According to [29], some dynamic properties have not been added to the model. For example, the floating particles in the ocean were not included in the simulation. Moreover, the model did not consider surface waves and their resulting light damping effect.

The precision of the visibility range was a limitation of this simulator. Though the attenuation factors were provided in the source code, they could change significantly with the water quality and backscattering of the underwater particles. Precise estimation of the visibility range was out of the scope of this paper. But, according to [30], a visibility range of around 10m was usually used for underwater vision systems.

As a result, the study used the visibility range estimate of 10 meters. The AUV was assumed to start the navigation process at a distance of less than 10m away from the underwater pipeline. When the AUV was released from the boat to start the mission, the GPS position was known. With the use of dead reckoning, the AUV maintained its position even after losing the GPS signal with increasing depth. A recent study of underwater dead reckoning [31] showed that the drift could be controlled to 5m over a time frame of two hours, making the assumption of having a drift amount less than the visibility range reasonable. Once the AUV reached the required depth, it searched for the pipeline.

The simulation world was composed of the "ocean box," the pipeline, and the AUV. The radius of the pipeline was 1 meter. To create a gradual turn, the pipeline was separated into four parts. Their size and positions are shown in Figure 1. The AUV used in the simulated environment had a dimension of $1.5(W) \times 2.6(L) \times 1.6(H) m^3$. It was spawned at a fixed depth of 90 meters. Apart from the essential components, several objects other than the pipeline were placed along the way to test the system's capability to identify the correct target. The setup of the virtual world is shown in Figure 2. To better simulate the complicated environment underwater, constant sea current was also applied to the simulation.

2) The software structure: The experiment was a closed-loop simulation system. The complete structure is shown in Figure 3. Using the current position of the AUV, the
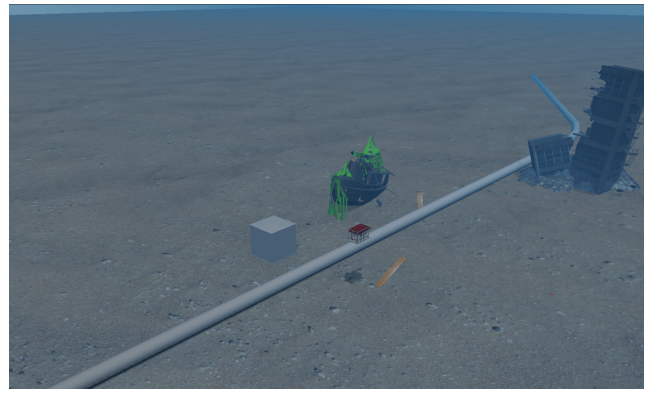

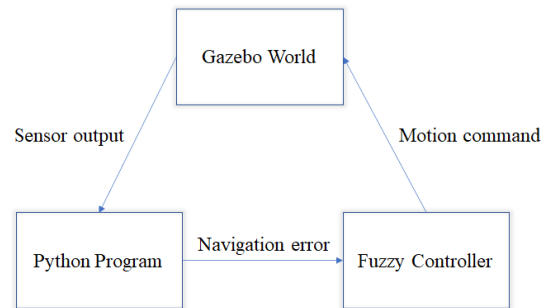Fig. 2. The simulated underwater world setup.

Fig. 3. The complete closed-loop structure of this research

ROS/Gazebo world simulated and reported the output from various sensors. With a self-developed Python program, current navigation errors were calculated and published to the ROS core. Additionally, the Fuzzy control module was utilized to send velocity commands to the AUV after making decisions according to the navigation errors.

B. The dynamic model of AUV

The position of the AUV was estimated using an Extended Kalman Filter (EKF). A derivation of 6 DoF (Degrees-of-Freedom) dynamic model with a simplification to 4 DoF was presented in [32].

The relation between the force from the thrusters and the velocity was expressed with the equation below

$$M\dot{v} + C(v)v + D(v)v + g(\eta) = \tau \qquad (2)$$

where M was the inertia of the AUV, $C(v)$ was the Coriolis effect matrix, $D(v)$ was the fluid drag matrix, and $g(\eta)$ was the acceleration sum of gravity and buoyancy, and η represented the vehicle position and pose. At the other side of the equation, τ represented the generalized force-torque vector exerted on the vehicle, including the force generated by the actuators, wind and the waves. Using the equation above, the state-space model was derived as

$$\begin{bmatrix} \dot{v} \\ \dot{\eta} \end{bmatrix} = \begin{bmatrix} M^{-1}\tau - M^{-1}(C(v) + D(v))v - M^{-1}g(\eta) \\ J(\eta)v \end{bmatrix} \qquad (3)$$

where J was the coordinate transformation matrix between the body frame and the global frame.
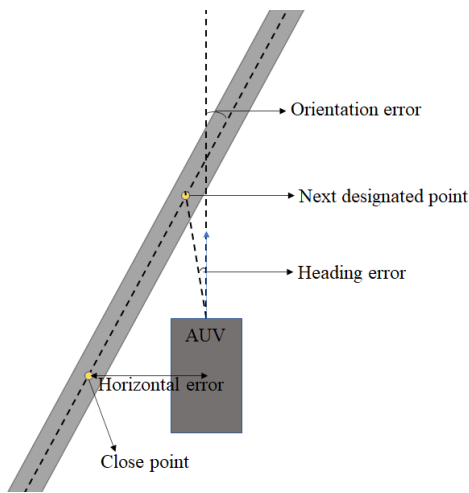
Fig. 4. Graphical explanation of orientation error, heading error and horizontal error in the proposed Fuzzy controller module
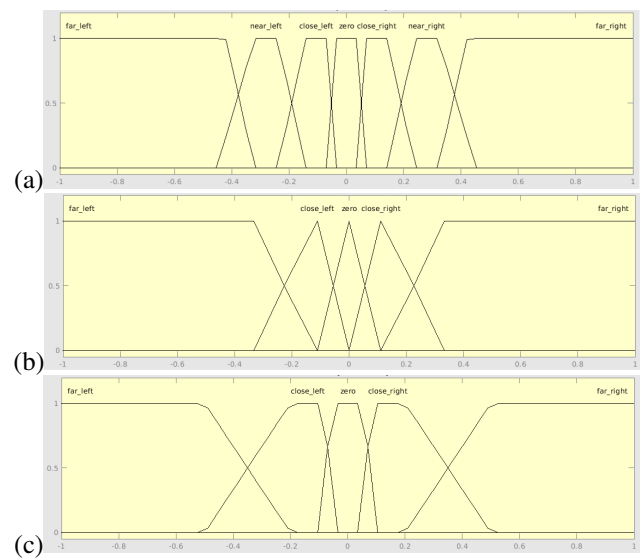

Fig. 5. Linguistic variable membership functions of the (a)heading error (b)horizontal error (c)orientation error

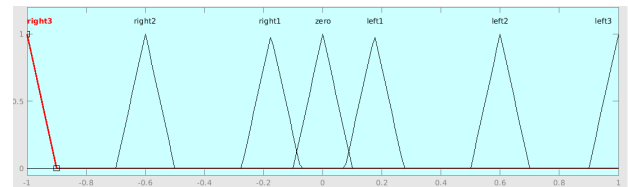Fig. 6. Defuzzification function of the fuzzy controller in this study

The velocity measurements in the EKF were collected from the DVL(Doppler Velocity Log) and the IMU(Inertial Measurement Unit) sensors, while the acceleration terms were derived by reading the force output from the eight thrusters on the AUV. With this dynamic model, the error of position estimation was around 0.7 meter. The detailed derivation is included in [32].

C. Fuzzy controller module

Fuzzy systems, also called expert systems, are constructed using the knowledge of experts. The system makes decisions with proper reasoning [33]. A rule-based fuzzy expert system was adopted for the proposed algorithm. One distinct advantage of the fuzzification process in fuzzy systems is in improving the noise tolerance in the underwater environment. The fuzzy control framework in [32] [34] was applied. The motion of the AUV was determined by analyzing three navigation errors - heading error, orientation error and horizontal error. The heading error was the angle difference between the current heading and the straight line from the AUV to the next designated point. The orientation error was the angle difference between the current heading and the pipeline's orientation. The horizontal error was the horizontal distance between the AUV and the pipeline. The graphical explanation of all three navigation errors is shown in figure 4.

According to the input values, the fuzzy control module evaluated the magnitude of all errors with their predefined linguistic variables (Figure 5). With the number of categories in each error, $5 \times 7 \times 5 = 175$ rules were expected in the rule base. To reduce the size, the hierarchical rule base reduction approach introduced in [34] and [35] was applied, reducing the number to 29. The rule base used in this study is presented in Table I. The final navigation decisions of the AUV were made accordingly.

The output value was then defuzzified according to the function in Figure 6. In this experiment, the angular velocity of the AUV was assigned according to the output value of the fuzzy controller with a fixed linear velocity of 0.15 m/s (forward).

D. Interpretations of visual and sonar data

In leveraging the fuzzy controller, the data retrieved from the camera and the sonar sensor was interpreted into the navigation errors.

1) Visual data: Two reference points mentioned in Figure 4 were analogized in the image data. Figure.7 is an example of the detected image. When a pipeline was present in the image, the middle point of the pipeline was analogous to the next designated point, and the pipeline's intersection with the bottom of the image was referenced as the close point.

Different from the original approach where a series of coordinate points are predefined, the "next designated points" and "close points" were updated with every incoming images in the proposed algorithm. Therefore, the resolution of the route was also increased, leading to a more precise navigation.

The reference points were translated from its image coordinates into vehicle coordinates through matrix transformation calculation considering the geometry and specifications of the camera system. Assuming the focal length of the camera was f, the image resolution was $H(height) \times W(width)$, and the camera was mounted at (x_0, y_0, z_0) with yaw angle of θ relative to the vehicle, the coordinate of the object relative to the camera was expressed as

$$x_c = \frac{(a - 2/W) \times z_c}{f sin(\theta)} \quad (4)$$

$$y_c = \frac{(b - 2/H) \times z_c}{f sin(\theta)} \quad (5)$$

TABLE I
RULE BASE OF THE FUZZY CONTROLLER IN THIS STUDY

| Horizontal error	Front angle error	Orientation error	Steering
Far left	Far left		Right3
Far left	Near left		Right2
Far left	Close left		Right1
Far left	Zero		Zero
Far left	Close right		Left1
Far left	Near right		Left2
Far left	Far right		Left3
Close left		Far left	Right3
Close left		Close left	Right2
Close left		Zero	Right1
Close left		Close right	Right1
Close left		Far right	Right1
Zero		Far left	Right2
Zero		Close left	Right1
Zero		Zero	Zero
Zero		Close right	Left1
Zero		Far right	Left2
Close right		Far left	Left3
Close right		Close left	Left2
Close right		Zero	Left1
Close right		Close right	Left1
Close right		Far right	Left1
Far right	Far left		Left3
Far right	Near left		Left2
Far right	Close left		Left1
Far right	Zero		Zero
Far right	Close right		Right1
Far right	Near right		Right2
Far right	Far right		Right3
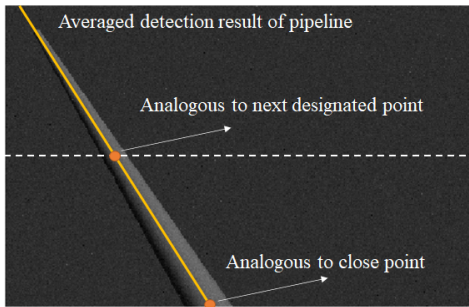
Fig. 7. An analogy was made between the image and physical space. The definition of next designated point and close point can be referred to Figure 4

$$z_c = \frac{h}{sin\theta + \frac{b-2/H}{f}cos\theta} \tag{6}$$

where h is the current distance between the vehicle and the ground.

A coordinate transform from image coordinates to AUV coordinates was then applied with the equation below.

$$\begin{bmatrix} X_v \\ Y_v \\ Z_v \end{bmatrix} = \begin{bmatrix} x_0 \\ y_0 \\ z_0 \end{bmatrix} + \begin{bmatrix} 0 & 0 & 1 \\ 0 & -1 & 0 \\ 1 & 0 & 0 \end{bmatrix} \begin{bmatrix} 1 & 0 & 0 \\ 0 & cos\theta & sin\theta \\ 0 & -sin\theta & cos\theta \end{bmatrix} \begin{bmatrix} x_c \\ y_c \\ z_c \end{bmatrix} \tag{7}$$

The three error values required for the fuzzy controller, horizontal error, front error and orientation error, were derived from the coordinates of the reference points. Assuming that the AUV coordinate of the next designated point
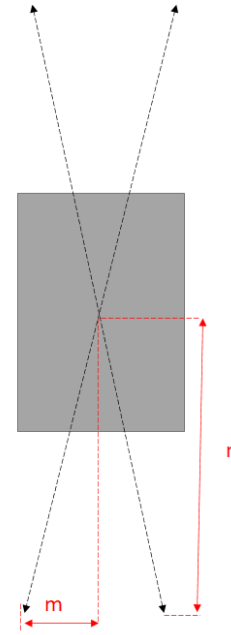

Fig. 8. Illustration of the sonar configuration on an AUV.

and the close point were derived to be $(x_{next}, y_{next}, z_{next})$ and $(x_{close}, y_{close}, z_{close})$, then the navigation errors were expressed as

$$E_{horizontal} = -y_{close}$$

$$E_{heading} = tan^{-1}\frac{y_{next} - y_{close}}{x_{next} - x_{close}} \tag{8}$$

$$E_{orientation} = tan^{-1}\frac{y_{next}}{x_{next}}$$

2) Sonar data: Horizontal error, heading error and orientation error can also be derived from the detected ranges from a 4-unit DVL sonar sensors. Assuming that the pipeline has a radius of r, the four sonar sensors are installed at the four corners of the AUV. The sensors are separated from each other at a distance of $2m$ from the left to the right side, and $2n$ from the front to the back. An illustration is shown in Figure. 8. Viewing from the top of the AUV, the sonar sensors detect the distance at four different directions. The four sonar sensors point toward the seabed slantingly. The end of the arrow represents the position where the sonar beam touches the ground.

Since the size of the pipeline and the distance from the vehicle to the ground were known values, distinguishing whether a single sonar sensor detected the pipeline was not difficult. According to the detection result of four sonar sensors, $2^4 = 16$ cases could be listed. And the navigation errors corresponding to each case were derived by averaging their probabilities.

When all four sonar sensors detected the pipeline, the averaged position/orientation of the vehicle is shown in Figure. 9(a). In this case, the navigation errors were

$$E[Error_{horizontal}] = 0 \tag{9}$$

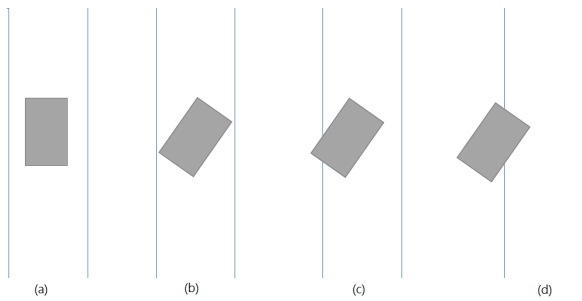$$E[Error_{orientation}] = E[Error_{heading}] = 0 \tag{10}$$

Fig. 9. Averaged position of the AUV when (a)all four sensors detected the pipeline (b)only the two diagonal sensors detected the pipeline (c)only one of the sensors did not detect the pipeline (d)only one of the sensors detected the pipeline.

The notation $E[\cdot]$ represented the expected value of the parameter inside the bracket.

When only the two diagonal sensors detected the pipeline, as shown in Figure. 9(b), the averaged condition led to the result

$$E[Error_{horizontal}] = 0 \tag{11}$$

$$E[Error_{orientation}] = E[Error_{heading}] = tan^{-1}(\frac{m}{n}) \tag{12}$$

In the case where the vehicle was horizontally flipped, that is, only the sensor at front-right and back-left detected the pipeline, the sign of the two angular errors were reversed.

If only one of the four sensors was out of the area of the pipeline, as shown in Figure. 9(c), the horizontal position relative to the pipeline had an offset to the left side. Therefore, the expected value of the errors were

$$E[Error_{horizontal}] = -0.5r \tag{13}$$

$$E[Error_{orientation}] = E[Error_{heading}] = tan^{-1}(\frac{m}{n}) \tag{14}$$

Similar calculation could be done on the case where the AUV was horizontally or vertically flipped.

In the last case shown in Figure. 9(d) where only one sonar sensor detected the pipeline, the AUV deviated from the pipeline at a larger distance than the previous cases. The expected value of the errors were

$$E[Error_{horizontal}] = -1.5r \tag{15}$$

$$E[Error_{orientation}] = E[Error_{heading}] = tan^{-1}(\frac{m}{n}) \tag{16}$$

Although the navigation errors in most of the cases could be estimated with the equations above, four special cases could not be successfully interpreted. When only two adjacent sonar sensors detected the pipeline, while the other two did not, the situation became indeterminate. One example is shown in Figure. 10. If only the two sensors at the front of the AUV detected the pipeline, the AUV could possibly be at the left or the right side relative to the pipeline. A similar situation was also found when only the sensor on the left/right/back side of the AUV detected the object. In these four cases, the navigation errors were not derivable. Under these circumstances, the image processing results were referred to for the navigation errors.
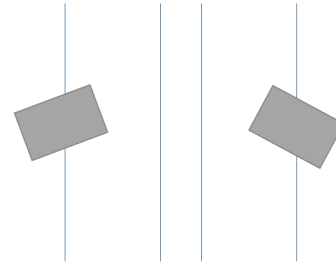

Fig. 10. Illustration of one of the indeterminate cases.

<div align="center">TABLE II</div>
<div align="center">NAVIGATION ERROR INTERPRETATION OF EVERY POSSIBLE DETECTION RESULT.</div>

1	2	3	4	$E_{heading}$	$E_{orientation}$	$E_{horizontal}$
+	+	+	+	0	0	0
+	+	+	-	$-tan^{-1}(m/n)$	$-tan^{-1}(m/n)$	$0.5r$
+	+	-	+	$tan^{-1}(m/n)$	$tan^{-1}(m/n)$	$-0.5r$
+	+	-	-	N/A	N/A	N/A
+	-	+	+	$tan^{-1}(m/n)$	$tan^{-1}(m/n)$	$0.5r$
+	-	+	-	N/A	N/A	N/A
+	-	-	+	$tan^{-1}(m/n)$	$tan^{-1}(m/n)$	0
+	-	-	-	$-tan^{-1}(m/n)$	$-tan^{-1}(m/n)$	$1.5r$
-	+	+	+	$-tan^{-1}(m/n)$	$-tan^{-1}(m/n)$	$-0.5r$
-	+	+	-	$-tan^{-1}(m/n)$	$-tan^{-1}(m/n)$	0
-	+	-	+	N/A	N/A	N/A
-	+	-	-	$tan^{-1}(m/n)$	$tan^{-1}(m/n)$	$-1.5r$
-	-	+	+	N/A	N/A	N/A
-	-	+	-	$tan^{-1}(m/n)$	$tan^{-1}(m/n)$	$1.5r$
-	-	-	+	$-tan^{-1}(m/n)$	$-tan^{-1}(m/n)$	$-1.5r$
-	-	-	-	N/A	N/A	N/A

Combining the results derived above, the navigation errors are represented in Table II. In this table, '+' represents 'detected' while '-' represents 'not detected'. The order of the sensors is front-left, front-right, back-left, back-right.

The interpreted navigation errors from both visual and sonar sensors were processed by the fuzzy controller, thereby navigating the AUV towards the predetermined route. This function was verified with a series of experiments done in a simulated environment.

E. Navigation in the simulated environment

The proposed navigation algorithm was applied on the simulated AUV. The detection data from the Gazebo world and the calculated navigation command was communicated through the ROS core of the system.

1) Image processing: The camera mounted on the simulated AUV had a resolution of 768×492 with 8-bit RGB depth. The camera was installed at a position of $(1.15, 0, 0.4)$ with respect to the AUV. Furthermore, the line of sight of the camera was tilted toward the ground at an angle of 0.6 rad. The sketch of the spatial relation between the AUV and camera is shown in Figure 11. The horizontal and vertical field of view of the camera were 124.2(deg) and 100.8(deg) respectively.
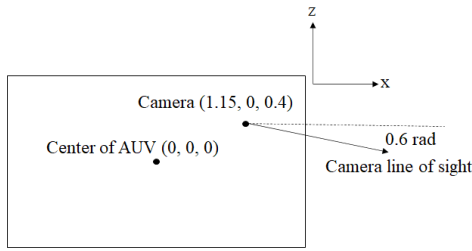
Fig. 11. Position and line of sight of camera relative to AUV

TABLE III
INSTALLATION DIRECTIONS OF SONAR SENSORS

Sensor#	Yaw	Pitch	Direction
1	-0.4	0.1	Front-left
2	-0.4	-0.1	Front-right
3	0.4	0.1	Rear-left
4	0.4	-0.1	Rear-right

TABLE IV
NAVIGATION ERROR INTERPRETATIONS FOR EVERY DETECTION RESULT.

1	2	3	4	$E_{heading}$	$E_{orientation}$	$E_{horizontal}$
+	+	+	+	0	0	0
+	+	+	-	-0.18	-0.18	0.5
+	+	-	+	0.18	0.18	-0.5
+	+	-	-	N/A	N/A	N/A
+	-	+	+	0.18	0.18	0.5
+	-	+	-	N/A	N/A	N/A
+	-	-	+	0.18	0.18	0
+	-	-	-	-0.18	-0.18	1.5
-	+	+	+	-0.18	-0.18	-0.5
-	+	+	-	-0.18	-0.18	0
-	+	-	+	N/A	N/A	N/A
-	+	-	-	0.18	0.18	-1.5
-	-	+	+	N/A	N/A	N/A
-	-	+	-	0.18	0.18	1.5
-	-	-	+	-0.18	-0.18	-1.5
-	-	-	-	N/A	N/A	N/A

After acquiring the image, an enhancement process was applied to the image. A detailed block diagram is shown in Figure 12. After the image was converted to grayscale, it went through a plateau histogram equalization [36] process with a threshold value of 10 to present an image with better contrast. A 3×3 median filter [37] was then applied to eliminate speckle noise from the environment. After noise reduction, a Sobel edge detection filter [38] was applied in the x and y direction on the image respectively. Since the simulated AUV was intended to cruise along the pipeline, the weights of the vertical edge is weighted more than horizontal edge. The ratio were set to be $2 : 1$. This weight adjustment enhanced the system's capability in recognizing the pipeline that aligned with the vehicle's direction.

After the image enhancement processes, a Hough transform [39] was applied to the image. 10 detected straight lines with the highest response were recorded. In order to represent the detected pipeline with one single line, the 10 recorded lines were averaged and expressed as

$$x_{img}cos\theta_{avg} + y_{img}sin\theta_{avg} = \rho_{avg} \qquad (17)$$

where θ_{avg} and ρ_{avg} were the average value of all 10 recorded lines. An example of the detection result is shown in Figure 13. In this figure, the red line represents 10 lines with the highest response and the yellow line represents their average.

The averaged pipeline detection results were then applied to the proposed algorithm (Equation (8)), deriving the appropriate motion commands.

2) Sonar processing: In the simulated AUV, a 4-unit sonar sensor was mounted at $(-1.4, 0, -0.312)$ relative to the vehicle. The 4 single sonar sensors were installed in different directions (Table III) with respect to the coordinate axis as shown in Figure 14.

The single sonar sensors returned the range measurements in the corresponding directions. With a fixed AUV depth, the sonar sensors' detection points were directly measured to be 0.64m from the vertical center line and 3.4m from the horizontal center line. A clear graphical description is shown in Figure 15.

Based on the sonar sensors' detection direction and the size of the underwater pipeline, the detected range was between 8.2m (center line of pipeline) and 10.4m (seabed.) Therefore, the detection threshold was set to be 8.5m. Any range value smaller than 8.5m was categorized as "detected".

With only four sonar sensors, precise navigation errors were not feasible. However, with the fuzzy controller and the proposed interpretation algorithm, precise navigation was achieved. Given the configuration of the simulated sonar system, Table IV provides the corresponding navigation errors under most cases. In this table, '+' represents 'detected' while '-' represents 'not detected'.

3) Sensor fusion: As discussed, four single sonar sensors could not provide navigation errors under all conditions. Moreover, the line detection algorithm was more susceptible to errors due to other objects and noise. The coordination between the camera and sonar sensors was beneficial for the navigation system.

Since the camera had a much larger field of view than the single sonar sensors, the camera was used in the initial search of the underwater pipeline. When the AUV was close enough to the pipeline, the sonar could cooperate with the camera and contribute to the navigation process. In this scenario, since the AUV was already approaching the pipeline, large errors that appeared suddenly were unlikely to be found. These large errors could have been a false alarm that came from other nearby objects. When the navigation errors from both sensors were present, the one with the smaller value was adopted. The fused navigation errors were then sent to the fuzzy controller for the motion control.
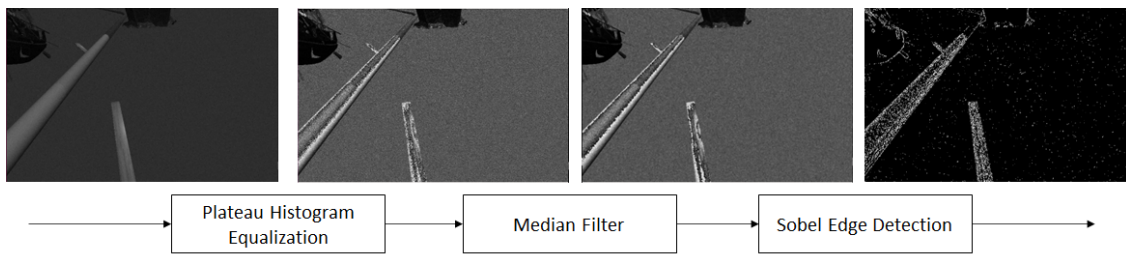
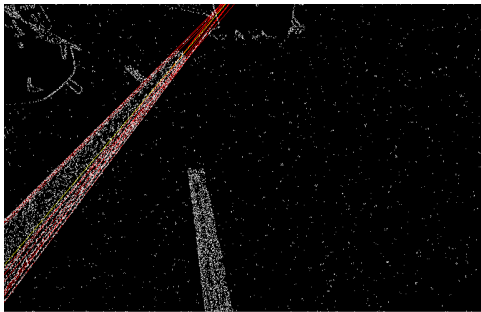Fig. 12.   Detailed block diagram of the image enhancement process

Fig. 13.   Example of the pipeline detection results.

F. Leak detection

A leak detection mission was implemented for further experimentation. A plume package developed by [40] was used to simulate a leaking pipeline. A random number of chemical particles were generated with random moving velocities. Each existing particle contributed to the concentration distribution function. A chemical particle concentration sensor detected the sum of the concentration distribution function and published it to the ROS core. Detailed derivations were included in [40] as well. The sensor was mounted on the AUV and reported the chemical concentration value with respect to the center of the AUV.

In this experiment, the leak point was set up at $(0, 0, -99)$. The position with the highest chemical concentration were recorded and reported after the inspection was finished. This point was marked as a leak point and reported to the users. Figure 16 shows the chemical concentration readout in one of the trials.

III. RESULTS

With the simulation environment setup as described in the method section, a series of experiments were conducted to
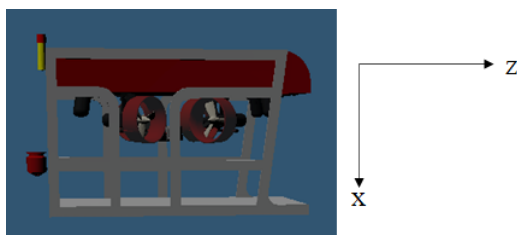

Fig. 14.   Detection direction of sonar was defined relative to the coordinate system shown in this figure

Fig. 15.   Detection point by direct measurement is shown in this figure. (Top view of the AUV)

verify the ability of the system to navigate and detect leaks.

The AUV was operated at a depth of 90m while the depth of the ocean was set to 100m. The current wave ranging from 0 to 1.2m/s was applied to the vehicle. The static optical effects and noise had been included in the simulation model. Detailed experimental results, errors and analysis are provided.

A. AUV navigation

In evaluating the system's abilities in navigation, the AUV's trajectory was measured while it navigated towards/along the pipeline. Its precision was assessed by the Root Mean Square(RMS) error of all points along the trajectory.

1) Pipeline following precision: In this experiment, the AUV was spawned on top of the pipeline at a coordinate of $(0, 0, -90)$ heading in the positive y direction. The trials were conducted under image-only and sensor fusion control schemes respectively. The RMS position error was 0.905 m (image-only) and 0.481 m (sensor fusion) respectively. The results showed that the navigation result was greatly improved by introducing the sonar sensor.

The improvement of navigation error mainly came from the turning part of the pipeline. Since the camera had a relatively
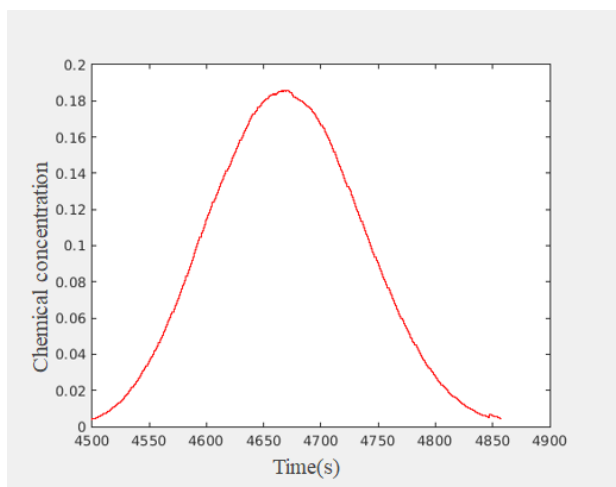
Fig. 16.   Example of chemical concentration measurement during a inspection mission in simulation environment
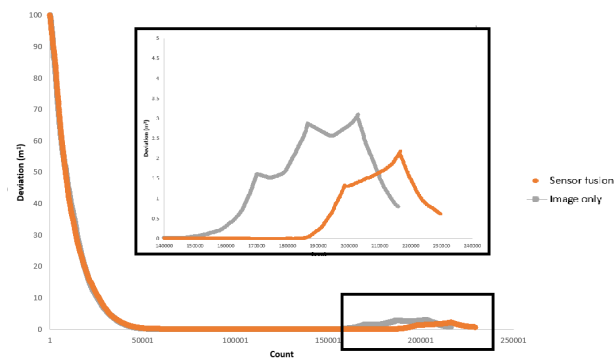

Fig. 17. Squared deviation of the trial

large field of view, the turning point ahead of the AUV was detected before reaching it. As a result, the AUV reacted to the turning point earlier than it should have, leading to a larger error. On the other hand, the sonar sensor only detected the pipeline 3.4m ahead and behind the AUV (see Figure 15). Therefore, the data retrieved from the sonar sensors navigation improved the turning precision. However, as shown in Table II, some of the conditions could not be interpreted with just sonar sensors. In addition, it was impossible to retrieve the pipeline once all four sensors lost track. As a result, a combination of sonar and image sensors was the best solution.

2) Pipeline approach precision: In this experiment, the AUV was spawned away from the pipeline at $(10, 0, -90)$ to evaluate the system's performance in approaching the pipeline. The squared deviation is shown in Figure 17 while the RMS trajectory error is provided in Table V. All position data during the experiment were plotted in order. The x-axis is the order while the y-axis shows the deviation value. The black frame shows where the pipeline turns.

From the measured results, it was observed that the AUV navigated towards the pipeline properly initially. However, an increased error could be found on the figure during the pipeline turn. Moreover, it was found that the proposed sensor fusion algorithm decreased the RMS error significantly when the AUV cruised along the bending part of the pipeline. This

RMS TRAJECTORY ERROR OF TWO TEST TRIALS THAT STARTED AWAY FROM THE PIPELINE.

Control type	Image-only	Sensor fusion
RMS error before turning (m)	2.610	2.539
RMS error during turning (m)	1.182	0.968
RMS error overall (m)	2.339	2.057

TABLE VI
RMS TRAJECTORY ERROR OF TEST TRIALS THAT STARTED AWAY FROM THE PIPELINE UNDER DIFFERENT LEVELS OF SEA CURRENT MAGNITUDES. (UNIT:M)

Sea current speed (m/s)	Image-only	Sensor fusion
0	2.339	2.057
0.4	2.439	2.272
0.7	2.465	2.292
1.0	2.493	2.390
1.2	2.514	2.470

result corresponded to the previous test where the AUV started on top of the pipeline. In conclusion, image data dominated the navigation when the AUV searched and approached the pipeline. Whereas, the inclusion of a sonar sensor helped the navigation system further decrease the error in trajectory when the AUV was cruising along the pipeline.

3) System robustness evaluation: In order to evaluate the system's robustness over a range of complex disturbances, a constant sea current of various magnitude was applied to the simulation environment. The setup of sea current magnitude followed [41]. Similar to the pipeline approaching experiment, the AUV was spawned at $(10, 0, -90)$. The coordinate of the vehicle was recorded compared with the ground truth, which was the coordinate of the pipeline.

The experimental result is shown in Table. VI. Though the navigation error increased with sea current speed, the AUV approached the pipeline and followed it. This successfully demonstrated the robustness of the navigation framework in noisy environments. In addition, a comparison between image-only and sensor fusion approaches are also provided in this table. A reduction in the navigation error resulted from the inclusion of sonar sensors.

4) Comparison to previous work: A comparison was performed between the proposed method and previous studies. With the input of the position data, study in [12] navigated the AUV to follow specific paths leveraging fuzzy logic. The measured navigation error was 1.02 and 1.09 m in two different trajectories. On the other hand, [9] used adaptive PID control and the GPS signal to navigate the AUV. A comb-shaped trajectory was chosen for the experiment. It was shown that the RMS error in the main part of the route was less than 1m. The work in [42] proposed using a proximity sensor to execute the pipeline following mission. The RMS error was approximately 2m when initialized on top of the pipeline.

Without relying on GPS data, the proposed navigation framework reached the same level of accuracy as the position-based algorithms. In addition, in the experiments where the

This article has been accepted for publication in IEEE Sensors Journal. This is the author's version which has not been fully edited and content may change prior to final publication. Citation information: DOI 10.1109/JSEN.2023.3250721

10   IEEE SENSORS JOURNAL, VOL. XX, NO. XX, XXXX 2022

TABLE VII
COMPARISON BETWEEN THE PROPOSED WORK AND PREVIOUS WORKS. (UNIT:M) (* APPROXIMATED FROM THE TRAJECTORY PLOT)

	Requires GPS	Path	Starting point	Error
[12]	Yes	tanh / spiral	4m away	1.02-1.09
Proposed	No	Segments	4m away	1.07m
[9]	Yes	Comb shape	on the path	< 2m *
[42]	No	Segments	on the path	< 2m *
Proposed	No	Segments	on the path	0.48m

TABLE VIII
EXPERIMENTAL RESULT OF THE LEAK DETECTION TEST.

P_{Start}	Heading	P_{Near}	$P_{Detection}$
(10,-20)	+y	(1.79, 0.35)	(1.16, 4.22)
(10,-25)	+y	(1.05, 0.16)	(0.75, 3.29)
(10,-30)	+y	(0.55, 0.07)	(0.39, 2.88)
(10,-35)	+y	(0.54, 0.01)	(0.49, 2.79)
(-10,-20)	+y	(-2.09, 0.38)	(-1.92, 1.34)
(-10,-25)	+y	(-1.44, 0.19)	(-1.15, 2.22)
(-10,-30)	+y	(-1.04, 0.09)	(-0.63, 3.12)
(-10,-35)	+y	(-0.77, 0.05)	(-0.52, 2.24)
(10,20)	-y	(1.94, -0.36)	(1.41, -3.61)
(10,25)	-y	(1.20, -0.16)	(0.87, -2.77)
(10,30)	-y	(0.64, -0.05)	(0.53, -1.38)
(10,35)	-y	(0.36, -0.01)	(0.30, -2.35)
(-10,20)	-y	(-2.07, -0.30)	(-1.65, -3.13)
(-10,25)	-y	(-1.37, -0.16)	(-1.10, -2.83)
(-10,30)	-y	(-0.98, -0.06)	(-0.80, -3.78)
(-10,35)	-y	(-0.76, -0.01)	(-0.73, -1.6)

AUV started on the designated path, the proposed algorithm significantly outperformed the previous work. The comparison table is shown in Table. VII.

B. Leak detection

To evaluate the system's performance in recognizing a leak point on the pipeline, the plume package mentioned previously was used to generate a virtual leak point. The plume source was set to be $(0, 0, -99)$. The AUV was spawned at 16 different points (P_{Start}) with a depth of 90m. The AUV was navigated towards the pipeline with the chemical concentration sensor. The points where the AUV was nearest to the plume source (P_{Near}) and where the AUV detected the highest chemical concentration ($P_{Detection}$) were recorded to evaluate the precision of leak detection. With the difference between the two points, an error was calculated to assess the performance of the leak detection. The experimental data is shown in Table VIII. In the table, P_{Start} is where the AUV was released. P_{Near} is where the AUV's position is nearest to the plume source. $P_{Detection}$ is where the largest chemical concentration was detected.

From the experimental data, it was found that the detected leak point had an error between 0.97 to 3.92m. The average error and standard deviation was 2.58 and 0.79(m) respectively. Apart from the magnitude of the errors, their direction was also

consistent. From the data, it was concluded that $P_{detection}$ was always found once the vehicle reached P_{Near}. The reason is that the plume source kept releasing chemical particles even after the AUV passed the point nearest to it. This caused a delay in the detection of leak points.

IV. CONCLUSION

In this study, a precise and cost-efficient way to conduct underwater pipeline inspection was demonstrated in a GPS-denied environment. All of the presented challenges in the underwater environment have been considered. With only a camera and four-unit sonar sensors, the AUV successfully navigated toward the pipeline and cruised along it with a precision that outperformed the previous studies. Additionally, with fuzzy logic included in the navigation framework, the robustness of the navigation framework was demonstrated under various current velocities. Finally, when using the proposed navigation system, it was shown that the AUV could achieve a much higher precision compared to the conventional leak detection sensors.

The navigation framework proposed in this study has shown great potential for application to autonomous underwater pipeline inspection. This method can also be translated to other vision systems working under environments with limited visibility.

In future research, the system's robustness for visibility variations and obstacles could be enhanced. For instance, including additional sensors into the fusion framework is promising. In addition, using adaptive parameters as inputs in image processing can help in significantly increasing the environmental tolerance of the system. Finally, the dynamic surface wave effects that were not included in the simulator can be determined through real-world experiments. A down-scaled AUV that can be tested in pools is currently under consideration.

REFERENCES

[1] J. Agbakwuru, "Oil/gas pipeline leak inspection and repair in underwater poor visibility conditions: Challenges and perspectives," *Journal of Environmental Protection*, vol. 03, 01 2012.

[2] M. A. Adegboye, W.-K. Fung, and A. Karnik, "Recent advances in pipeline monitoring and oil leakage detection technologies: Principles and approaches," *Sensors*, vol. 19, no. 11, 2019. [Online]. Available: https://www.mdpi.com/1424-8220/19/11/2548

[3] N. Mohamed, I. Jawhar, J. Al-Jaroodi, and L. Zhang, "Sensor network architectures for monitoring underwater pipelines," *Sensors*, vol. 11, no. 11, pp. 10 738–10 764, 2011. [Online]. Available: https://www.mdpi.com/1424-8220/11/11/10738

[4] I. Jawhar, N. Mohamed, J. Al-Jaroodi, and S. Zhang, "An architecture for using autonomous underwater vehicles in wireless sensor networks for underwater pipeline monitoring," *IEEE Transactions on Industrial Informatics*, vol. 15, no. 3, pp. 1329–1340, 2019.

[5] C. Mai, S. Pedersen, L. Hansen, K. L. Jepsen, and Z. Yang, "Subsea infrastructure inspection: A review study," in *2016 IEEE International Conference on Underwater System Technology: Theory and Applications (USYS)*. IEEE, 2016, pp. 71–76.

[6] M. Jacobi and D. Karimanzira, "Underwater pipeline and cable inspection using autonomous underwater vehicles," in *2013 MTS/IEEE OCEANS - Bergen*, 2013, pp. 1–6.

[7] Y. Wu, X. Ta, R. Xiao, Y. Wei, D. An, and D. Li, "Survey of underwater robot positioning navigation," *Applied Ocean Research*, vol. 90, p. 101845, 2019. [Online]. Available: https://www.sciencedirect.com/science/article/pii/S0141118718305546

[8] X. Xiang, B. Jouvencel, and O. Parodi, "Coordinated formation control of multiple autonomous underwater vehicles for pipeline inspection," *International Journal of Advanced Robotic Systems*, vol. 7, no. 1, p. 3, 2010. [Online]. Available: https://doi.org/10.5772/7242

[9] Y. Li, Y.-q. Jiang, L.-f. Wang, J. Cao, and G.-c. Zhang, "Intelligent pid guidance control for auv path tracking," *Journal of Central South University*, vol. 22, no. 9, pp. 3440–3449, 2015.

[10] S. A. Fjerdingen, E. Kyrkjeboe, and A. A. Transeth, "Auv pipeline following using reinforcement learning," in *ISR 2010 (41st International Symposium on Robotics) and ROBOTIK 2010 (6th German Conference on Robotics)*, 2010, pp. 1–8.

[11] H. Hai, Z. Guocheng, Q. Hongde, and Z. Zexing, "Autonomous underwater vehicle precise motion control for target following with model uncertainty," *International Journal of Advanced Robotic Systems*, vol. 14, no. 4, p. 1729881417719808, 2017. [Online]. Available: https://doi.org/10.1177/1729881417719808

[12] X. Xiang, C. Yu, and Q. Zhang, "Robust fuzzy 3d path following for autonomous underwater vehicle subject to uncertainties," *Computers & Operations Research*, vol. 84, pp. 165–177, 2017. [Online]. Available: https://www.sciencedirect.com/science/article/pii/S0305054816302374

[13] E. Trabes and M. A. Jordan, "A node-based method for slam navigation in self-similar underwater environments: a case study," *Robotics*, vol. 6, no. 4, p. 29, 2017.

[14] W. Remmas, A. Chemori, and M. Kruusmaa, "Diver tracking in open waters: A low-cost approach based on visual and acoustic sensor fusion," *Journal of Field Robotics*, vol. 38, no. 3, pp. 494–508, 2021.

[15] G. Foresti, "Visual inspection of sea bottom structures by an autonomous underwater vehicle," *IEEE Transactions on Systems, Man, and Cybernetics, Part B (Cybernetics)*, vol. 31, no. 5, pp. 691–705, 2001.

[16] C.-C. Cheng and B.-T. Jiang, "A robust visual servo scheme for underwater pipeline following," in *2012 19th International Conference on Systems, Signals and Image Processing (IWSSIP)*, 2012, pp. 456–459.

[17] G. Allibert, M.-D. Hua, S. Krupiński, and T. Hamel, "Pipeline following by visual servoing for autonomous underwater vehicles," *Control Engineering Practice*, vol. 82, pp. 151–160, 2019. [Online]. Available: https://www.sciencedirect.com/science/article/pii/S0967066118306312

[18] A. Ortiz, M. Simó, and G. Oliver, "A vision system for an underwater cable tracker," *Machine vision and applications*, vol. 13, no. 3, pp. 129–140, 2002.

[19] Y. Liu, F. Wang, Z. Lv, K. Cao, and Y. Lin, "Pixel-to-action policy for underwater pipeline following via deep reinforcement learning," in *2018 IEEE International Conference of Intelligent Robotic and Control Engineering (IRCE)*. IEEE, 2018, pp. 135–139.

[20] Y. Song, J. Qian, R. Miao, W. Xue, R. Ying, and P. Liu, "Haud: A high-accuracy underwater dataset for visual-inertial odometry," in *2021 IEEE Sensors*, 2021, pp. 1–4.

[21] O. Calvo, A. Sousa, A. Rozenfeld, and G. Acosta, "Smooth path planning for autonomous pipeline inspections," in *2009 6th International Multi-Conference on Systems, Signals and Devices*. IEEE, 2009, pp. 1–9.

[22] B. Mitchell, N. Mahmoudian, and G. Meadows, "Autonomous underwater pipeline monitoring navigation system," in *Automatic Target Recognition XXIV*, vol. 9090. International Society for Optics and Photonics, 2014, p. 90900D.

[23] A. Bagnitsky, A. Inzartsev, A. Pavin, S. Melman, and M. Morozov, "Side scan sonar using for underwater cables & pipelines tracking by means of auv," in *2011 IEEE Symposium on Underwater Technology and Workshop on Scientific Use of Submarine Cables and Related Technologies*. IEEE, 2011, pp. 1–10.

[24] O. Calvo, A. Sousa, A. Rozenfeld, and G. Acosta, "Smooth path planning for autonomous pipeline inspections," in *2009 6th International Multi-Conference on Systems, Signals and Devices*. IEEE, 2009, pp. 1–9.

[25] M. Jacobi and D. Karimanzira, "Multi sensor underwater pipeline tracking with auvs," in *2014 Oceans-St. John's*. IEEE, 2014, pp. 1–6.

[26] G. C. Karras, P. Marantos, C. P. Bechlioulis, and K. J. Kyriakopoulos, "Unsupervised online system identification for underwater robotic vehicles," *IEEE Journal of Oceanic Engineering*, vol. 44, no. 3, pp. 642–663, 2019.

[27] G. Billings, R. Camilli, and M. Johnson-Roberson, "Hybrid visual slam for underwater vehicle manipulator systems," *IEEE Robotics and Automation Letters*, pp. 1–1, 2022.

[28] G. G. Acosta, O. A. C. Ibanez, H. J. Curti, and A. F. Rozenfeld, "Low-cost autonomous underwater vehicle for pipeline and cable inspections," in *2007 Symposium on Underwater Technology and Workshop on Scientific Use of Submarine Cables and Related Technologies*, 2007, pp. 331–336.

[29] M. M. M. Manhães, S. A. Scherer, M. Voss, L. R. Douat, and T. Rauschenbach, "Uuv simulator: A gazebo-based package for underwater intervention and multi-robot simulation," in *OCEANS 2016 MTS/IEEE Monterey*, 2016, pp. 1–8.

[30] J. C. Kinsey, R. M. Eustice, and L. L. Whitcomb, "A survey of underwater vehicle navigation: Recent advances and new challenges," in *IFAC conference of manoeuvering and control of marine craft*, vol. 88. Lisbon, 2006, pp. 1–12.

[31] Z. Yan, S. Peng, J. Zhou, J. Xu, and H. Jia, "Research on an improved dead reckoning for auv navigation," in *2010 Chinese Control and Decision Conference*, 2010, pp. 1793–1797.

[32] A. Rajput, "Steering control and kalman filter position estimation comparison for an autonomous underwater vehicle," Master's thesis, Dept. Systems. Eng., University of Illinois at Urbana-Champaign, IL, 7 2021.

[33] S.-H. Liao, "Expert system methodologies and applications—a decade review from 1995 to 2004," *Expert systems with applications*, vol. 28, no. 1, pp. 93–103, 2005.

[34] W. R. Norris, *A design framework for qualitative human-in-the-loop system development*. University of Illinois at Urbana-Champaign, 2001.

[35] J. Xu and W. R. Norris, "Hierarchical fuzzy control design and stability analysis for steering-control based vehicles," in *Proceedings of the 2019 4th International Conference on Automation, Control and Robotics Engineering*, 2019, pp. 1–7.

[36] V. E. Vickers, "Plateau equalization algorithm for real-time display of high-quality infrared imagery," *Optical engineering*, vol. 35, no. 7, pp. 1921–1926, 1996.

[37] W. K. Pratt, *Digital Image Processing*. New York: Wiley, 1978.

[38] I. Sobel and G. Feldman, "A 3x3 isotropic gradient operator for image processing," *a talk at the Stanford Artificial Project in*, pp. 271–272, 1968.

[39] P. V. Hough, "Method and means for recognizing complex patterns," Dec. 18 1962, uS Patent 3,069,654.

[40] Y. Tian and A. Zhang, "Simulation environment and guidance system for auv tracing chemical plume in 3-dimensions," in *2010 2nd International Asia Conference on Informatics in Control, Automation and Robotics (CAR 2010)*, vol. 1, 2010, pp. 407–411.

[41] C. Chen, S. Shiotani, and K. Sasa, "Effect of ocean currents on ship navigation in the east china sea," *Ocean Engineering*, vol. 104, pp. 283–293, 2015.

[42] P. K. Paim, B. Jouvencel, and L. Lapierre, "A reactive control approach for pipeline inspection with an auv," in *Proceedings of OCEANS 2005 MTS/IEEE*. IEEE, 2005, pp. 201–206.

I-Chen Sang received Bachelor's degree and Master's degree in Physics from National Tsing-Hua University in 2014 and 2016. Having five years of experience in the optoelectrical industry as a systems engineer, she is currently pursuing the Ph.D. degree in the Systems Engineering program at the University of Illinois Urbana-Champaign. She is working as a Research Assistant in the Autonomous and Unmanned Vehicle Systems Laboratory (AUVSL), founded by Prof. William R. Norris. Her focus includes the navigation of autonomous vehicles, sensor fusion, and image processing using fuzzy logic.

William R. Norris received BS (1996), MS(1997), and Ph.D.(2001) degrees in systems engineering from the University of Illinois Urbana-Champaign and holds an MBA (2007) from The Fuqua School of Business at Duke University. He has over 23 years of industry experience with autonomous systems. Prof. Norris is currently a Clinical Associate Professor in the Industrial and Enterprise Systems Engineering department at the University of Illinois Urbana-Champaign, director of the Autonomous and Unmanned Vehicle System Lab (AUVSL) as well as the founder and director of the Center of Excellence for Autonomous Construction and Manufacturing at Scale (CEACaMS).